UNIVERSIDAD DISTRITAL FRANCISCO JOSÉ DE CALDAS

REVISTA UD Y LA GEOMÁTICA

http://revistas.udistrital.edu.co/ojs/index.php/UDGeo/index
http://dx.doi.org/10.14483/udistrital.jour.udgeo.2014.9.a06

UD y la GEOMÁTICA

INVESTIGACIÓN

Remote Detection of Oil Slicks at the Ocean Surface

Detección remota de petróleo en la superficie del océano

Sonia C. Gallegos[1], Oscar Garcia-Pineda[2], William Pichel[3], Nickolai Kukhtarev[4], Tatiana Kukhtareva[5], Duane Armstrong[6]

Citación / Gallegos, S.C., Garcia-Pineda, O., Pichel, W., Kukhtarev, N., Kukhtareva, T., & Armstrong, D. (2014). UD y la Geomática. (9) pp 57-65

Fecha de recepción: 30 de septiembre de 2014. **Fecha de aceptación:** 29 de noviembre de 2014.

ABSTRACT

The 2010 Deepwater Horizon (DWH) oil slick caused by the explosion of the Macondo well was the worst man-made disaster in the history of the Gulf of Mexico, and the largest marine spill in the history of the petroleum industry. We provide an overview of our efforts to monitor the extent of these slicks using automated algorithms for the Moderate Resolution Imaging Spectroradiometer (MODIS), and the Synthetic Aperture Radar (SAR). We discuss the advantages and limitations of each of the methods in detection of oil from space, and suggest that the NIR bands may be the best option to monitor emulsified oil when using passive sensors. Additionally, we discuss current laboratory-based efforts to measure oil thickness via holographic interferometry, and propose this as an ideal technique for future remote sensing of oil.

Key words: detection of petroleum, interferometry, lasers, MODIS, SAR

RESUMEN

El derrame de petróleo causado por la explosión del pozo petrolero Macondo y conocido con el nombre de Deepwater Horizon (DWH) o el Horizonte de Aguas Profundas, fue el peor desastre causado por el hombre en la historia del golfo de México, así como el derrame marino más grande en la historia de la industria petrolera. Presentamos un resumen de nuestros esfuerzos para detectar y monitorear la extensión del derrame automáticamente, usando datos del radiómetro espectral de resolución moderada (MODIS) y del radar de apertura sintética (SAR). Así mismo, discutimos las ventajas y las limitaciones de cada uno de los métodos en la detección de petróleo. Sugerimos que las bandas del infrarojo cercano (NIR) son la mejor opción para monitorear emulsiones de petróleo con sensores pasivos. Además, relatamos nuestros esfuerzos de laboratorio para medir el espesor de la capa de petróleo, y proponemos que esta es una técnica ideal para implementarse en futuros sensores remotos.

Palabras clave: detección de petróleo, interferometría, láseres, MODIS, SAR

[1] Naval Research Laboratory /NASA – ASTPO John C. Stennis Space Center, MS 39529, sonia.gallegos@nrlssc.navy.mil
[2] Florida State University /EOAS 600 W College Ave, Tallahassee, FL 32306, ogarciapineda@fsu.edu
[3] NOAA/STAR 5830 University Research Court College Park, MD 20740, william.g.pichel@noaa.gov
[4] Alabama A & M University Normal, AL 35762 nickoly.kukhtarev@aamu.edu
[5] Alabama A & M University Normal, AL 35762 Tanja.kukhtareva@aamuu.edu
[6] NASA-ASTPO Stennis Space Center, MS 39529 Curtis.d.armstrong@nasa.gov

1. Introduction

Oil, oil wastes, and general petroleum contamination pose environmental risks to the Gulf of Mexico waters. Primary inputs come from oceanic transportation and tanking, recreational activities, ship/platform and coastal facilities spills, oil exploration, atmospheric deposition, and non-point sources derived from human activities on land (National Research Council [NRC]., 2003, p.16). The Gulf of Mexico (GOM) is particularly vulnerable to oil contamination because it is a semi-enclosed basin, which receives the industrial waste of 87.3 million people who live in its drainage basin (Broadus & Vartanov, 1994, p. 24). It is also the sixth largest hydrocarbon basin of the world, which produces 23% (roughly 10 million cubic feet per day) of the USA gas production and 30% (1.5 million barrels per day) of its oil production. The GOM and Outer Continental Shelf (OCS) contains approximately 3,800 fixed platforms that extract hydrocarbons constantly. 2,000 of those are large platforms and 1,000 are constantly manned. These are connected to the mainland by 37,000 miles of pipelines. With 42 million acres under lease, and many more deep water platforms expected to be constructed in the near future, the GOM oil leaks are bound to increase. Gas and oil leakage are inherent casualties of the business of extracting oil. Even if these were to be totally controlled, oil and gas seeps naturally at the bottom of the Gulf reach the surface intermittently. They have been estimated to cover approximately ~850 sq. km and ~150 sq. km of the northern and southern Gulf, respectively (MacDonald *et al.,* 1996). Those from the northern Gulf yield about 140,000 tons per year (Kvenvolden & Cooper, 2003, p. 143).

In spite of the constant danger of petroleum leakage, there are currently no means to monitor the leakages on an operational basis. Agencies usually take action after oil slicks are reported by individuals, ships or airplanes. Our goal was to initiate the building of a system that could automatically detect the presence of oil in imagery of the Moderate Resolution Spectral Radiometer (MODIS) and the Synthetic Aperture Radar (SAR). Our effort started one year prior to the DWH oil spill occurrence. The data which became available to the project from this occurrence enhanced our work and enabled us to expand into laboratory work, which would not have been feasible otherwise. In this paper, we present the results of our initial and current efforts on oil slick detection.

2. Methods

The first approach relies on the remote identification of oil slicks using mathematical tools such as edge detectors, polygon algorithms and neural networks in both the MODIS and SAR data. The second approach includes laboratory analyses to characterize oil and non-oiled water via interferometric holography.

2.1 The MODIS Algorithm

Passive sensors such as the Moderate Resolution Imaging Spectroradiometer (MODIS), are not an ideal for oil detection, but their data are highly desirable because of their coverage frequency. The visible channels, in particular cannot differentiate oil under nadir or near-nadir conditions because of the absence of a spectral signature specific for oil. Oil is easily detected in the sunglint portion of the swath where the specular reflectance of the sun over the ocean surface is a function of the oceanic surface slope (Hu, Li, Pichel, & Muller-Karger, 2009, p.1). The reflectance at the sea surface was first described and quantified by (Cox & Munk, 1954, p. 838). In this classic work, they showed that the sea surface could be represented by a collection of mirror-like planar surfaces, each having a characteristic slope. The probability that a facet reflects specularly the incident radiation from the sun to the sensor depends on the wind speed and direction, and sea state. Oil on the surface of the ocean reduces the surface slope and modifies the sensors acquisition geometry. Thus, the oil patch appears bright amidst a less illuminated surface. The amount of energy received at the sensor is also a function of the thickness of the oil patch. Heavy crude oil will absorb much of the radiation and return a reduced signal, while thinner layers may not be able to drastically change the ocean slope, and not be detected at all. Figure 1 presents A MODIS image under sun glint conditions, the bright reflectance in the middle of the Gulf belong to the DWH oil spill.

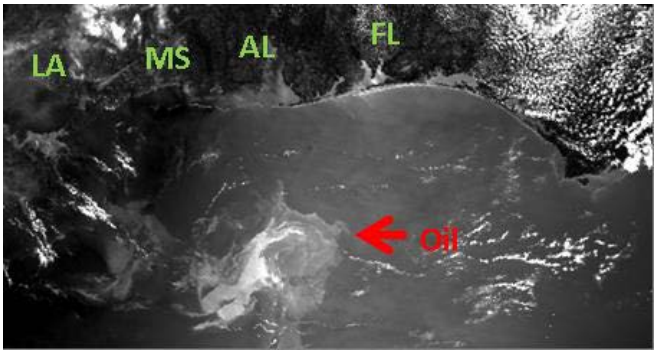

Figure 1. MODIS imagery of the NE Gulf of Mexico for May 17, 2010. Bright pixels in the center belong to the DWH oil slick.

The MODIS algorithm consists of edge detection, edge sealing and polygon algorithms. It is a modified version of an algorithm previously developed by (Gallegos, Hawkins & Cheng, 1993) to identify and remove clouds in data from the Advanced Very High Resolution Radiometer (AVHRR). Because the oil pool is only apparent in the glinted imagery, the algorithm is applied to the specular reflectance of the MODIS visible bands. The first step in the edge detection procedure requires the computation of the Gray Level Co-Occurrence (GLC) matrix. The (i,j)th element of the matrix is the relative frequency of occurrence of gray

level i and gray level j when separated by a distance or displacement vector (Δx, Δy) within a window or local neighborhood of size M x N.

Given a range of intensity levels from 0 to L-1, the GLC matrix is calculated from

$$P(i,\ j)|(\Delta x,\ \Delta y) = \sum_{n-1}^{N-\Delta y} = 1 \sum_{m=1}^{M-\Delta x} A$$

where,

$$A = \frac{1}{(M-\Delta x)(N-\Delta y)}$$

If *f(m,n)* =1 and *f(m+x, n+ y)* =j, a=0 otherwise *f(m,n)* is the intensity level of the pixel at sample m, line n of the window.

For this specific study, the size of the local neighborhood (window) was initially set to 3 x 3 pixels separated by a distance Δx = 1 , and Δy= 1. The small window size and displacement vector was chosen to allow the smallest changes in intensity to be detected over small distances. The computations of the GLC matrix result in a second-order probability matrix of size L x L from which the cluster shade, a measure of the local variation in intensity between pixels, is calculated for each local neighborhood.

$$S\ (\Delta x,\ \Delta y) = \sum_{i=0}^{L-1} L-1 \sum_{j-0} (i + j - \mu_i - \mu_j)^3 P(i,j) \mid \Delta x, \Delta y$$

Where,

μi and μj are estimates of mean intensity calculated from the weighted summations of rows and columns of the matrix:

$$\mu i = \sum_{i0}^{L-1} i \sum_{j-0}^{L-1} P(i, j \mid \Delta x, \Delta y)$$

$$\mu i = \sum_{j=0}^{L-1} i \sum_{i=0}^{L-1} P(i, j \mid \Delta x, \Delta y)$$

These computations produce a new image in which the center of each neighborhood is replaced with a cluster shade value. Edges are produced at the site of the neighboring pixels whose cluster shade values are opposite in sign (zero crossing) and where both have cluster shade intensities greater or equal to a chosen threshold. The default threshold is 3. This value is altered to adjust the computation and the generation of edges to larger and more distinguishable targets.

After the zero crossing test most of the edges are in place. However, some of these occur as isolated strings which are not attached to other edges. To enable these strings to join other strings, new thresholds and conditions for edge forming are set. For an array to enter the new computations, its center pixel must be greater or equal than a new threshold. The default threshold is 1. The procedure can be repeated as many as 17 times. Both the threshold and the repetition times can be altered to suit the needs of the target detection. Edge pixels are = 0, and non-edge pixels = 1.

The algorithm exploits differences in radiances to create edges. Heterogeneous waters produce large number of edges and homogenous few edges. After the zero crossing test most of the edges are in place. However, this simple edge detection is insufficient to identify targets because some edges occur as isolated strings. To remove the strings or to join them with other larger and most significant strings, which may or may not be part of a target of interest, a new zero-crossing test is implemented. The default threshold is 1. 3x3 arrays or windows of non-edge pixels are examined. For an array to qualify for this test its center must be greater or equal than the new threshold and one of its pixels must be an edge pixel. New edges are generated at the site of those pixels whose value is greater than and opposite in sign to the new threshold. The procedure can be repeated as many times as desired. To avoid excessive computation a number passes between 10 and 25 is desirable. The default value is 17.

The result of this last computation is a binary image which contains areas of non-edge pixels surrounded by edge pixels. Initially, each line of data is screened for contiguous non edge pixels. Upon encountering the beginning of a string in a cluster of non-edge pixels, the algorithm assigns it a unique 16-bit identification number. It continues to search for other contiguous non-edge pixels until the entire scene is segmented into clusters separated from each other by edges. Because this procedure generates large number of clusters, some of which may be noise, the very small clusters are eliminated from consideration if the number of non-edge pixels in the cluster is smaller than the number of pixels in its edge boundary. Then statistics are run on the pixels on either side of the edge surrounding the cluster. For a cluster to be considered "useful" the inside pixels must have a value equal or higher than the outside pixels. Glinted water has higher reflectance than non-glinted water.

A modified version of the algorithm was applied to nadir and near nadir MODIS near-infrared bands (NIR) centered at 1.24 μm (band 5). At NIR wavelengths greater than 0.8 μm, seawater is highly absorbent, and the water leaving radiance is assumed to be negligible (black pixel). Although this is quite true of open waters, it is not so for coastal waters where sediment and other particulates have signals at these wavelengths. Additionally, floating vegetation (i.e., *Sargassum* spp.) and thick and emulsified oil can be observed at NIR wavelengths, due to their backscattering

properties. During the DWH oil spill, (Clark *et al.*, 2010) measured the reflectance of fresh oil at NIR wavelengths under laboratory conditions, and indicated that detection of oil over water was a function of the oil: water ratio, and oil thickness could be estimated from diagnostic organic C-H absorptions centered at 1.20 um, 1.73 um, and 2.37 um (Fig 2).

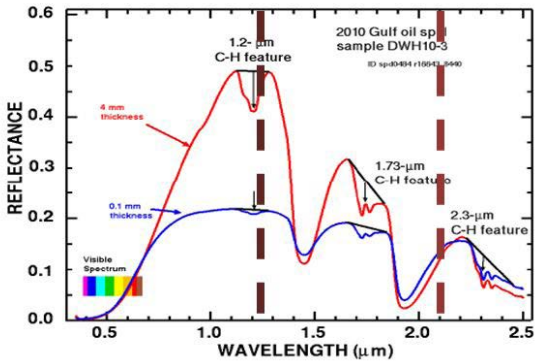

Figure 2: Oil reflectance after Clark *et al.* (2010). The vertical broken lines depict the approximate location of MODIS band 5 (1.24 mm) and band 7 (2.13 mm).

In this figure, oil thickness is calculated from the difference between the shoulders and the bottom of the indentations in the spectra. (Clark *et al*, 2010, p.13) applied their laboratory findings to the data of the Airborne Visible/Infrared Spectrometer (AVIRIS) for estimating oil thickness and volume of oil spilled, with a high level of success. The estimations were mostly for surface oil since light penetrates only micrometers in the NIR.

The MODIS bands that approximate the oil diagnostic bands are centered at 1.24μm and 2.13μm, neither of which could be used to estimate oil thickness. In spite of this, the thick and emulsified oil, which tends to form clumps and float at the surface of the water, has a reflectance different from that of the surrounding clear waters. It provides a unique opportunity to test edge detection algorithms. For this effort, we used a modified version of the algorithm previously described for sun glinted MODIS data. The polygon algorithm was modified to accept a minimum reflectance of 2, and a minimum number of pixels within a polygon (cluster) of 400.

2.2 The SAR Oil Mapping Algorithm

The ability of SAR to detect features at the ocean's surface depends on the interaction between the SAR pulse of microwave energy and the sea-surface. The radar return from contrasting roughness components of the sea surface, which ranges from capillary waves to short gravity waves produce characteristic patterns in the radar imagery (Holt & Hillarnd, 2000). Ocean slicks are a subset of ocean features detected in SAR data. They are areas of distinctly contrasting brightness against the radar backscatter produced by wind-generated Bragg waves at length scale of ~1 to 10cm. SAR shows the reflectivity of the sea surface in radar frequencies, which is significantly decreased in the presence of slicks which damp capillary surface waves. SAR data suffers from many false alarms associated with fresh water slicks, calm winds which tend to generate flat surfaces, wave shadows behind land or structures, submerged weed beds, and organic exudates from marine organisms, which produce signatures similar to those of oil slicks under calm wind conditions (Fingas & Brown, 2014).

The methodology used with the SAR data included a modified version of a Feed-Forward Neural Network (FFNN) classification method, known as the Textural Classifier Neural Network Algorithm (TCNNA), developed by (Garcia-Pineda, MacDonald & Zimmer, 2008, p.1265) which has 46 inputs, 5 hidden layers and a log-sigmoid transfer function at the output layer (Figure 3). Outputs are either 0= no slick, and 1= slick.

This method has been successful at extracting targets (oil seeps) and rapidly interpreting images collected under a wide range of environmental conditions. Interpreted images produce binary arrays with imbedded geo-reference data that are easily stored and manipulated in GIS software. The TCNNA was tuned for larger spills during the DWH spill. It uses SAR data and wind parameterizations from the CMOD model, which provides the backscattering coefficient according to wind speed, wind direction, and incidence angle. The algorithm relies on two neural nets (NN). The first is a mask which identifies and isolates 'oil-like' pixels in the imagery based on their backscattered energy, incidence angle, and wind speed. The results of the first NN feed into the second. The second NN performs a statistical textural classification on the 'oil-like' pixels. For the classification, it relies in bounding arrays centered on the pixel to be classified. The arrays are 21x21 or 51x51 pixels, which are used to remove non-oil pixels at different spatial resolutions. Texture measures such as average, smoothness, third moment, entropy and uniformity are computed for each of the arrays. Of these, the measurements with the highest weights on the classification are third moment and entropy. The results are binary files with values 0 for non-oil and 1 for oil. The output of the TCNNA algorithm is a binary image that can be converted into a polygon layer in a GIS program.

2.3 Laboratory Experiments

Neither field collections nor laboratory experiments were planned for the original effort on oil detection. Nevertheless, it would have been a missed opportunity not to observe the oil slicks, and to collect and analyze samples. The *in situ* collections which entailed measuring oil reflectance

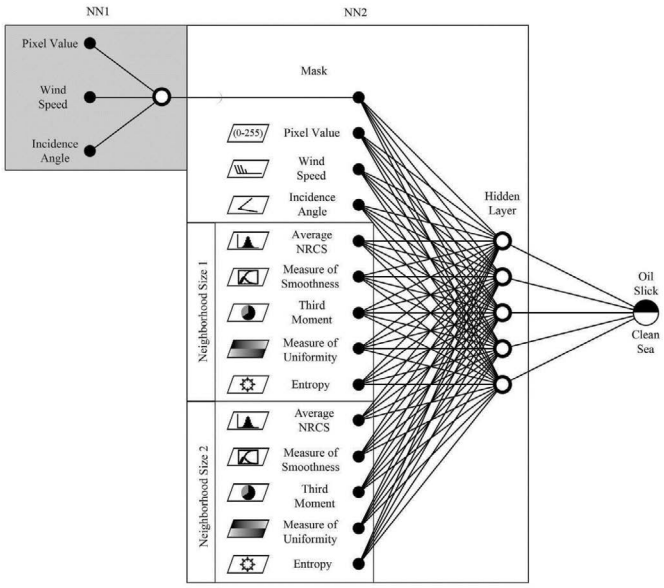

Figure 3. Architecture of the Textural Classifier Neural Network Algorithm

with a field radiometer did not yield new insights into the behavior of the oil at visible wavelengths. The laboratory experiments, which relied on holographic interferometry produced interesting results. Samples were collected from areas of fresh petroleum located approximately five miles away from the Macondo well in the Gulf of Mexico. The samples were stored in dark bottles, sealed and maintained on ice in dark coolers until shipped. Water samples from areas not impacted by the oil were also collected, filtered with a GFF filter, and stored in the same manner as the oil. Upon reaching the laser laboratories at Alabama A & M University, a sample of both oil and filtered seawater or CDOM was placed in small shallow containers for interferometric measurements. The scheme used for measurement appears in Figure 4.

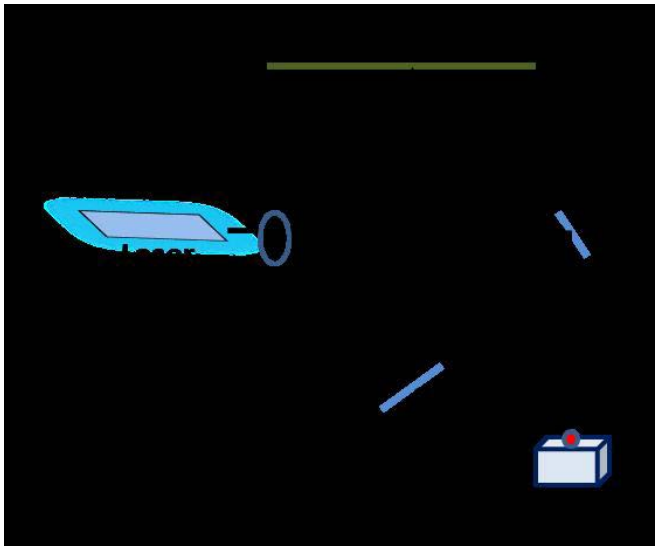

Figure 4. Scheme used for holographic interferometric measurements

In this figure, a beam from an HE-Ne laser (0.632 μm) passing through a lens (F= 5cm) was shined onto a sample of oil-on-water or filtered sea water. The instantaneous field of view for the oil was ~12 cm and that for the seawater was ~4 cm in diameter. The beams reflected from the top and bottom of the sample formed interference patterns. These were projected onto the screen, which was placed 3 m away from the samples. The patterns were photographed from the screen.

3. Results

Testing of the algorithm on oil seeps from the Gulf of Mexico and on the DWH oil slicks revealed that it performs well at the edges of the sun glint pool, which is the most difficult task in this type of identification. An example of its performance on the oil seeps can be viewed in Figure 5. In this Figure, thin slicks one or two pixels (~2km) in width cannot readily be detected because of the threshold values. There is a trade-off between identifying the large pools and leaving outside the thin lines, or identifying the thin lines and misidentifying large portions of the oil pool. How much of the oil pool is identified depends on the oil:water ratio, and whether or not there is enough contrast between pixels to obtain a stable edge, that does not get removed by the polygon algorithm.

Clouds and cloud shadows pose a major problem to the identification of oil in sun glinted imagery. The high and cold clouds have similar reflectance as those of the bright pixels in the oil-contaminated sun glint pool. Cloud shadows introduce dark spots, which end up producing texture in the water, where it does not exist. Until a more accurate cloud masking technique can be found for MODIS data,

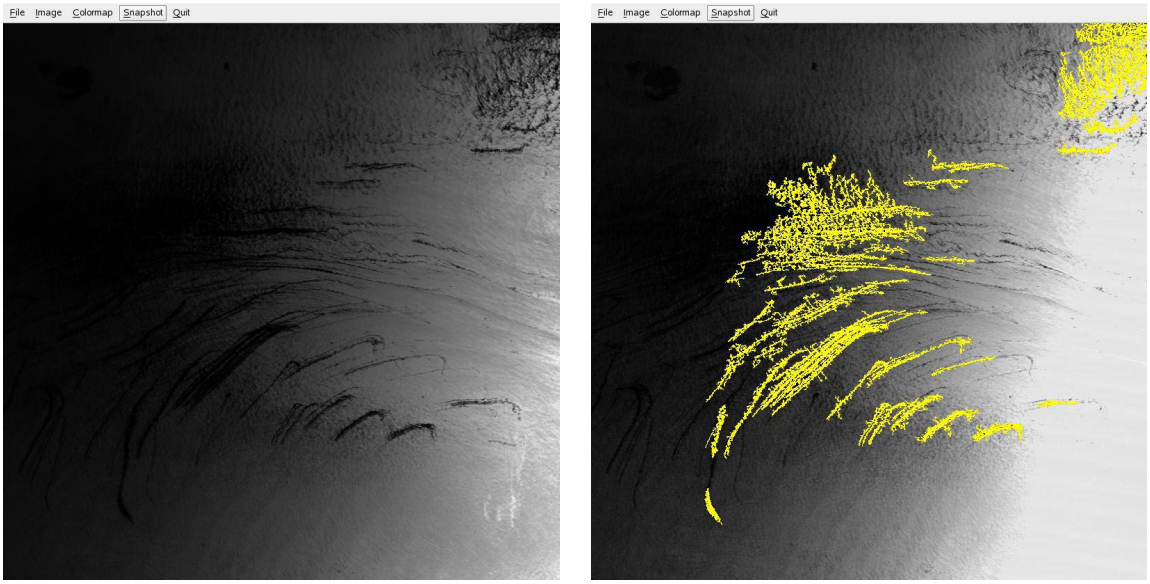

(a) (b)

Figure 5. (a) Oil slicks apparent in the sunglint of MODIS imagery (b) The same oil slicks overlaid by the result of the MODIS algorithm (yellow pixels).

the algorithm designed to identify oil plumes in its glinted imagery works only on cloud free scenes,

The initial results of the MODIS algorithm testing on the 1.24 μm NIR imagery is presented below. Figure 6a depicts the southern portion of the Mississippi River Delta. The large dark feature to the right of it belongs to the DWH oil spill as it appeared on May 23, 2010. Figure 6b shows the entire Mississippi sound, where land is identified by the red pixels, and clouds as the gray pixels. The oil pool, identified by the MODIS oil algorithm, appears as the large black and white textured feature between the Mississippi Delta and the parenthesis drawn in the scene for reference purposes. Other black and white areas around the coast are misinterpretations of the algorithm, which will have to be corrected in future versions. This portion of the MODIS algorithm is still a work in progress.

The most successful identification of oil pools from space was obtained with the TCNNA algorithm on SAR data. Although the algorithm does not perform as well on large oil pools as it does on the smaller seeps, it is without a doubt an excellent oil detection tool. The performance of this algorithm on SAR data is presented in Figure 7. A more

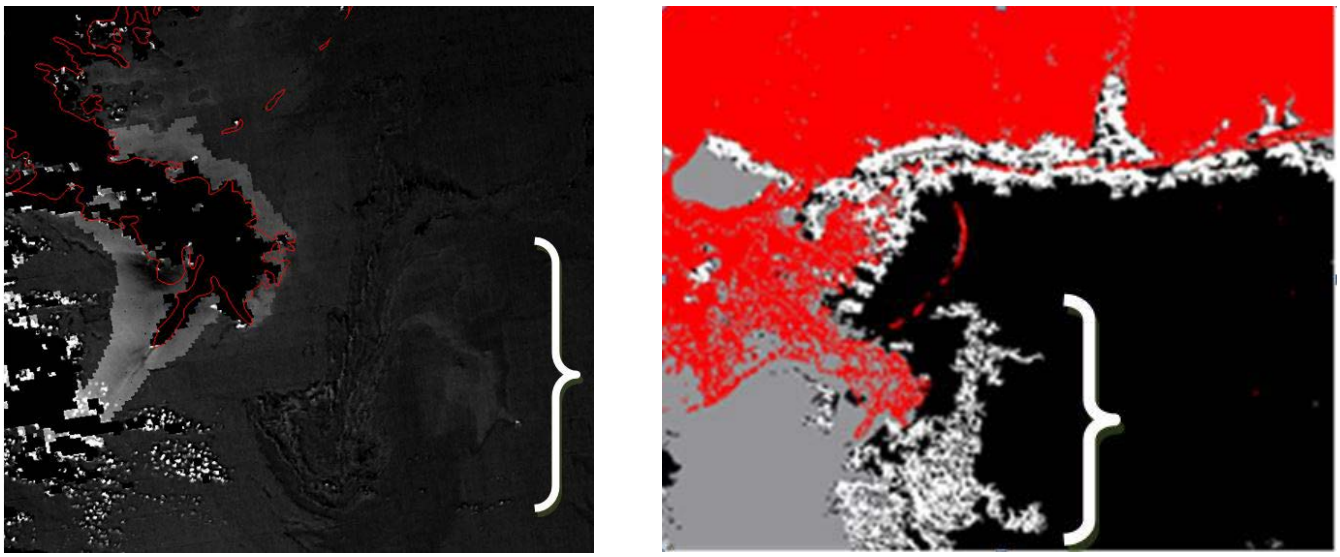

(a) (b)

Figure 6. (a) The Mississippi River Delta. Gray colors are oil and sediment mixture, black mass to the right is oil. (b) Oil identified by MODIS algorithm is white textured feature next to the parenthesis.

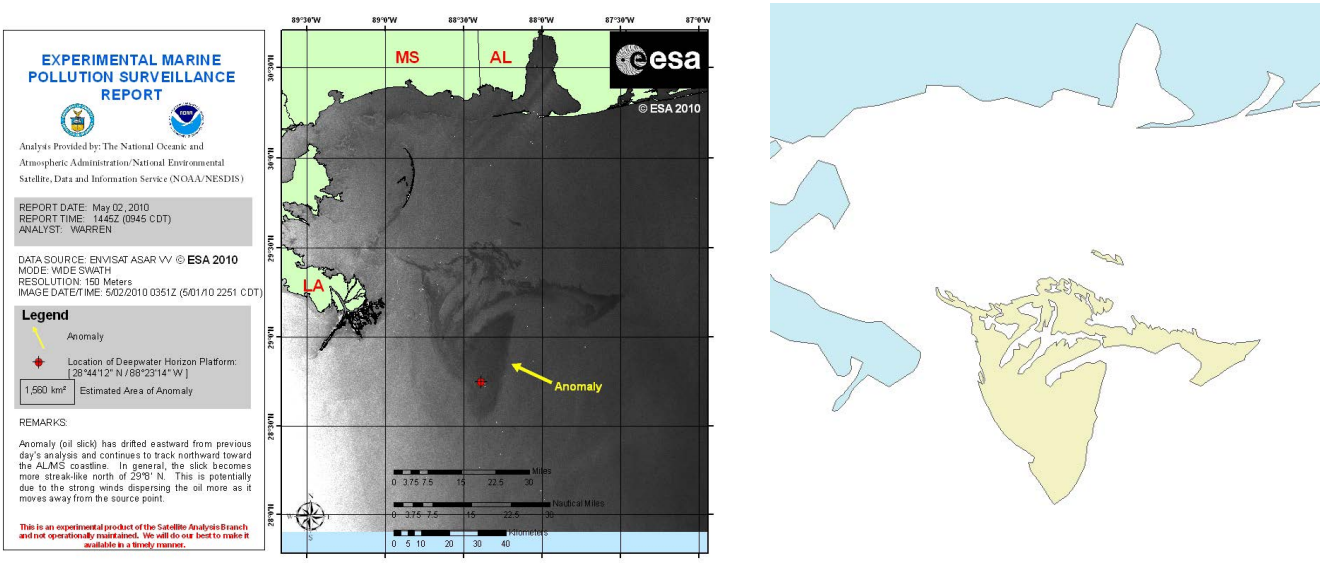

(a) (b)

Figure 7. (a) An oil slick observed by SAR on May 2, 2010, (b) Results of the TCNNA.

in-depth description of the TCNNA algorithm performance during the DWH oil spill can be found in Garcia-Pineda *et al.,* (2013).

Figure 7a presents one of the Experimental Marine Pollution Surveillance Reports, created by NOAA to monitor the displacement of the DWH oil slicks. The Report has a description panel on the left and a SAR image for May 2, 2010 on the right. The dark shades on the water indicate low backscattering due to oil. The location of the Macondo well is denoted by the red dot. Figure 7b shows a shape file which was produced when the binary image resulting from the TCNNA algorithm was converted into a polygon layer by a GIS program. Notice the close resemblance of the oil features in both the SAR and the shape file.

The holographic interference patterns using a HeNe red laser enabled the characterization of both samples, oil-on-water and filtered sea water or CDOM. The holographic interference pattern was produced by the interference of the wave reflected from the oil surface and wave reflected from the water on which the oil was floating. The results from the interferometric work appear in Figure 8. In this figure, clear water appears as black and the CDOM and oil

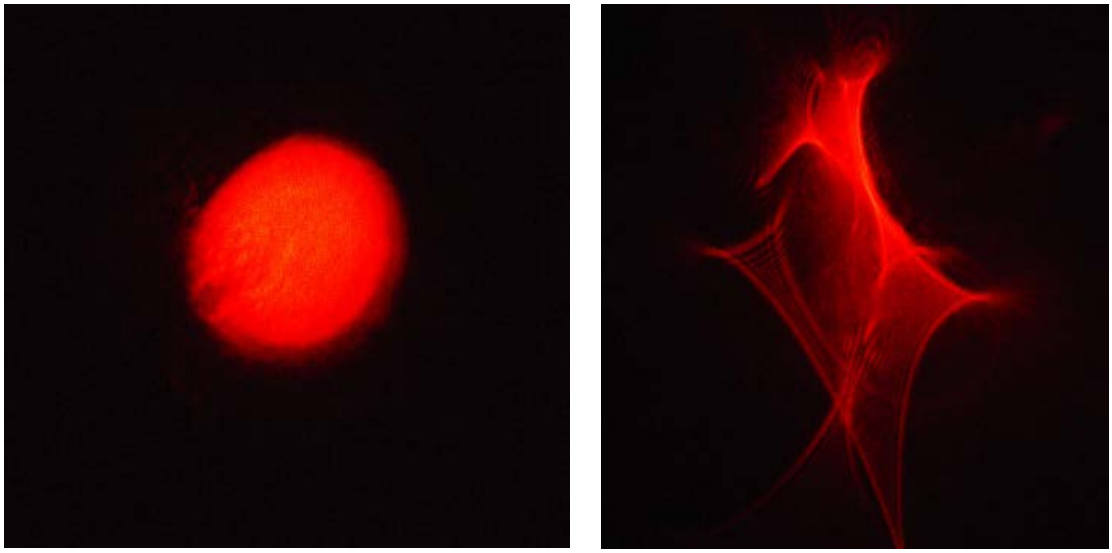

(a) (b)

Figure 8. (a) Interference pattern of (CDOM) (IFOV= 4 cm); (b) Interference pattern of crude oil in water (IFOV= 12 cm). Screen distance is 3 m for both.

appear as red. Figure 8a shows the interferometric pattern of CDOM, which appears flat with some structure but no fringes. Conversely, Figure 8b, which belongs to the oil has many fringes and a distinct shape. Estimates of oil thickness can be accomplished by counting the number of fringes on the interferograms and multiplying these by the laser wavelength (0.633 μm).

The fringes are created when the droplet of water spreads over the water surface. They are the result of interference between the reflected beam of light from the front surface of the oil and a plane wave reflected from the surface water.

4. Conclusions

It became apparent during the DWH oil spill that in spite of the many space sensors currently flying, none of them could provide accurate quantitative assessments needed for petroleum slick containment and for assessment of the ecological impacts of the spill. MODIS in spite of its daily data acquisition could only provide useful data during sun glint. SAR data was constrained by its 30 m resolution, wind, and other artifacts that confound the interpretation of the data. Oil thickness, the most important parameter in an oil spill could only be estimated from the surface film at NIR wavelengths from the Airborne Visible / Infrared Imaging Spectrometer (AVIRIS), flown in a different and separate effort by NASA/Jet Propulsion Laboratory.

The analyses performed by our group for the MODIS and SAR data did not expand the capabilities for detection of these sensors. They only automated the identification of oil-like features, which currently are manually obtained. The MODIS algorithm can outline the edge of an oil slick in the glinted image of visible channels as long as the oil slicks are thicker than 2 pixels. The adapted MODIS algorithm for the NIR band at 1.24 μm identifies with high accuracy the thick and emulsified oil, exclusively. Sediment-laden coastal waters, such as those of the Mississippi Sound challenge the performance of the algorithm because of their high reflectance. We are currently, devising methodology to separate the sediment laden texture from that of the oil in the MODIS algorithm. Clouds and cloud shadows pose major problems for the sunglint and the NIR analyses, which may or may not be solved during the course of this investigation.

The TCNNA algorithm for SAR performs extremely well on oil seeps, but it needs manual removal of some of the polygons (false positives) that are created during the identification of large oil pools. In spite of this, the TCNNA, which has been developing since 2007, is ready for operational work. It was transferred to NOAA/Satellite Analyses Branch (SAB) in 2011.

The interferometric work had interesting results and relevance to oil spill detection from space. It demonstrated that this method can identify oil thickness, and separate this signal from that of CDOM in the ocean. An ideal space sensor for oil detection would be one that combines fluorescence spectroscopy and interferometry for oil characterization. Such sensor does not currently exist, but we suggest that it is needed and should be planned for future space missions.

Acknowledgments

The authors would like to thank the NASA/Applied Science Program, and in particular, Dr. John Haynes, our project Manager. We extend our gratitude to the NASA Chief Technology Officer at John C. Stennis Space Center, Dr. R. Pelletier-Travis for supporting the laboratory efforts.

References

Broadus, J. & Vartanov, R. (1994). *The Oceans and Environmental Security: Shared US and Russian Perspectives*. Washington: Island Press.

Clark, R., Swayze, G., Leifer, I., Livo, K., Kokaly, R., Hoefen, T. Dominguez, R. (2010). A method for quantitative mapping of thick oil spills using imaging spectroscopy. U.S. Geological Survey Open-File Report 2010–1167, 51 p.

Cox, C. & Munk, W. (1954). Measurement of the Sea Surface from Photographs of the Sun's Glitter. *Journal of the Optical Society of America*, 44, (11), 838-850. DOI: 10.1364/JOSA.44.000838

Fingas, M. & Brown, C. (2014). Review of oil spill remote sensing. *Marine Pollution Bulletin* 83, 9-23. DOI: doi:10.1016/j.marpolbul.2014.03.059

Gallegos, S., Hawkins, J. & Cheng, C. (1993). A New Method of Cloud Masking for Advanced Very High Resolution Radiometer Full Resolution Data Over the Ocean. *Journal of Geophysical Research*, 98, (5), 8505-8516. DOI: 10.1029/93JC00100

Garcia-Pineda, O., MacDonald, I., Zimmer, B. (2008). Synthetic Aperture Radar Image Processing using the Supervised Textural-Neural Network Classification Algorithm. *Geoscience and Remote Sensing Symposium, 2008. IGARSS 2008. IEEE International*, 4, 1265-1268. DOI: 10.1109/IGARSS.2008.4779960

Garcia-Pineda, O. MacDonald, I., Li, X., Jackson, C. & Pichel, W. (2013). Oil Spill Mapping in the Gulf of Mexico with Textural Classifier Neural Network Algorithm (TCNNA). *Selected Topics in Applied Earth Observations and Remote Sensing, IEEE Journal of*, 6, (6), 2517-2525. DOI: 10.1109/JSTARS 20132244061

Holt, B. & Hilland, J. (2000). Rapid Repeat SAR Imaging of the Ocean Surface: Are Daily Observations Possible? *John Hopkins APL Technical Digest*, 4, (1), 162-169.

Hu, C., Li, X., Pichel, W. & Muller-Karger, F. (2009). Detection of Natural Oil Slicks in the NW Gulf of Mexico using MODIS imagery. Geophys. *Research Letters*, 26, (1), 1-5. DOI: 10.1029/2008GL036119, 2009

Kukhtarev, N., Kukhtareva, T. & Gallegos, S. (2011). Holographic Interferometry of oil films and droplets in water with single-beam mirro-type scheme. *Applied Optics*, 50, (8), 853-857. DOI: 10.1364/AO.50.000B53

Kvenvolden, K. & Cooper, C. (2003). Natural Seepage of Crude Oil Into the Marine Environment. *Geo-Mar Letters,* 23, 140-146. DOI: 10.1007/s00367-003-0135-0

MacDonald, I., Reilly, J., Best, S.,Venkataramaiah, R., Sassen, S., Guinasso, L...Amos, J. (1996). Remote sensing inventory of active oil seeps and chemosynthetic communities in the northern Gulf of Mexico. In D. Schumacher & M. Abrams (Eds.). *Hydrocarbon migration and its near-surface expression*. (pp. 27-37). Tulsa: The American Association of Petroleum Geologists.

National Research Council (NRC) (2003). *Oil in the Sea III Inputs, Fates and Effects*. Washington: The National Academies Press.